

Theory of dopants and defects in Co-doped TiO₂ anatase

James M. Sullivan and Steven C. Erwin

Center for Computational Materials Science, Naval Research Laboratory, Washington, D.C. 20375

(Dated: February 1, 2008)

We report first-principles microscopic calculations of the formation energy, electrical activity, and magnetic moment of Co dopants and a variety of native defects in TiO₂ anatase. Using these results, we use equilibrium thermodynamics to predict the resulting carrier concentration, the average magnetic moment per Co, and the dominant oxidation state of Co. The predicted values are in good agreement with experiment under the assumption of O-poor growth conditions. In this regime, a substantial fraction of Co dopants occupy interstitial sites as donors. The incomplete compensation of these donors by substitutional Co acceptors then leads to *n*-type behavior, as observed experimentally.

PACS numbers: PACS numbers:75.50.Pp,71.55.-i,61.72.Bb

I. INTRODUCTION

The recent discovery of room temperature ferromagnetism in Co-doped TiO₂ anatase¹ has led to a great deal of activity both to understand the origins of ferromagnetic order in this material and to raise the magnetic ordering temperature.^{2,3,4,5,6,7,8,9} One promising line of inquiry is to understand first the role of dopants and native defects in the TiO₂ host. For example, the location of Co dopants in this material (substitutional versus interstitial), their oxidation state, and their magnetic properties have been the subject of intense scrutiny.^{2,3,4,6,8} Furthermore, it has been suggested that O vacancies, which are believed to give rise to the observed *n*-type behavior in pure TiO₂ anatase,¹⁰ may provide free electrons which mediate the exchange interaction between the Co dopants.^{3,4} This possibility is very different from the hole mediated exchange interactions which are believed to describe ferromagnetic order in a wide variety of other dilute magnetic semiconductors, including InMnAs, GaMnAs, and MnGe,^{11,12,13} and may have a direct bearing on the origin of the anomalously high Curie temperature observed in Co-doped TiO₂ anatase.

In this paper, we first use density-functional theory to determine the electronic structure, formation energy, and electrical activity of Co dopants and several native defects in TiO₂ anatase. (In the remainder of this paper we will use “defects” to refer to both Co dopants and native defects.) We then use standard methods to calculate, as a function of temperature, the concentrations of each defect in the TiO₂ host over a range of Co and O chemical potentials relevant to different growth conditions. In summary, we find that O vacancies do not play any significant role in Co-doped anatase. Moreover, we find that the observed *n*-type behavior in Co-doped TiO₂ strongly suggests that roughly half of the total Co content is in interstitial sites. Under these conditions we find an enhancement—relative to the Co²⁺ low spin state—of the average value of the local magnetic moment, in good agreement with experiment. Finally, under these conditions essentially all of the of Co—both interstitial and substitutional—occurs in oxidation state II, as observed

experimentally.

II. BACKGROUND

We begin by briefly reviewing the relevant experimental results for Co-doped TiO₂ anatase. We concentrate solely on experimental results for samples in which Co is believed to be homogeneously distributed; hence, we do not address Co clustering or its consequences. We focus on three observations which show good experimental reproducibility: (1) the electrical nature of the samples (insulating versus *n*-type or *p*-type), (2) the Co oxidation state, and (3) the average magnetic moment per Co dopant.

Although the original work of Matsumoto and coworkers estimated the ferromagnetic ordering temperature to be larger than 400 K, the average magnetic moment per Co and *n*-type carrier concentration were modest, 0.32 μ_B and 10¹⁸/cm³ respectively. More recent efforts have led to a larger magnetic moment per Co of 1.26 μ_B ,^{2,3,4} and to *n*-type carrier densities of 10¹⁹/cm³.¹⁴ These increased values are likely due to improvements in sample quality achievable with oxygen plasma-assisted molecular-beam epitaxy (OPMBE).¹⁵ For example, these samples were well characterized to rule out Co inclusions as a source of the ferromagnetism.^{4,14} Using both Co 2*p* photoemission and Co K-shell x-ray absorption near-edge structure (XANES), the Co dopants in TiO₂ anatase were shown to have a formal oxidation state of II. A strong correlation between the magnetic and transport properties was demonstrated: both highly doped and highly resistive samples are typically non-magnetic, consistent with a picture of carrier-mediated ferromagnetism competing with an antiferromagnetic superexchange interaction.^{4,14}

III. THEORY

A. Formalism

To understand the role of defects in TiO_2 anatase, we initially adopt a simple picture of isolated impurities. In this approach, we first determine the energy required for the defect to form in a given charge state. We then use a standard thermodynamic approach to determine the expected concentration of such defects at a given temperature. We assume that the defects do not interact, except indirectly via charge transfer between them. Thus, for example, we do not address the origin of the apparent ferromagnetic coupling between Co dopants.

The defects we consider in this work are: interstitial Co (Co_{int}), substitutional Co on the Ti site (Co_{Ti}), O vacancies (V_{O}), interstitial Ti (Ti_{int}), and defect complexes consisting of nearest-neighbor pairs of substitutional Co and O vacancies ($\text{Co}_{\text{Ti}}\text{V}_{\text{O}}$). There are two crystallographically distinct types of such complexes: a $\text{Co}_{\text{Ti}}\text{V}_{\text{O}}$ pair oriented along the c -axis and a $\text{Co}_{\text{Ti}}\text{V}_{\text{O}}$ pair oriented nearly in the ab plane. We refer to these as $\text{Co}_{\text{Ti}}\text{V}_{\text{O}}\text{-}c$ and $\text{Co}_{\text{Ti}}\text{V}_{\text{O}}\text{-}ab$, respectively.

We make no assumptions about which defects are donors and which are acceptors, whether they are neutral or charged, or how many are actually present. At a given temperature, the concentration of each defect (in a given charge state) will be determined by its formation energy. We use density-functional theory in a supercell approach to calculate these formation energies according to

$$E_{\text{form}}^q = E_t^q - \sum_j n_j \mu_j + qE_F, \quad (1)$$

where E_t^q is the total energy of a supercell containing one defect in charge state q ; n_j and μ_j are the number and chemical potential (energy per atom in the ground-state phase) of each atomic species in the supercell; and E_F is the Fermi energy, measured with respect to the valence band maximum (VBM) of the host.^{16,17,18,19,20} Although the Fermi energy appears to be an independent variable here, it is in fact determined by the constraint of electroneutrality, as described below. Also, we note that although the total energies on the right-hand side of Eq. 1 depend on whether all-electron or pseudopotential methods are used, the formation energy itself is analogous to a binding energy, and can therefore be accurately calculated within either method.

In thermal equilibrium, the concentration of each defect, D , is determined by its formation energy:

$$C_D^q = N_{\text{sites}} \exp(-E_{\text{form}}^q/k_B T), \quad (2)$$

where N_{sites} is the number of sites per unit volume available to the defect. Since the formation energies depend on the chemical potentials and the Fermi level, it is evident that the concentrations also depend on these quantities. The concentrations must also satisfy the constraint

of overall electrical neutrality; this provides an additional equation that we use to determine E_F for any given choice of chemical potentials. The electroneutrality condition must take into account the contributions not only from charged defects, but also from p and n (the hole and electron carrier densities). Thus, for each given choice of the oxygen chemical potential, μ_{O} , and cobalt chemical potential, μ_{Co} , the following equation must be numerically solved:

$$p(E_F) - n(E_F) + \sum_{D,q} qC_D^q(E_F; \mu_{\text{O}}, \mu_{\text{Co}}) = 0. \quad (3)$$

Here, the sum is over all defects, D , in all possible charge states, q . The Ti chemical potential does not enter explicitly into this equation for reasons discussed in the following section, and, of course, the Co chemical potential is only relevant for defects involving Co. The carrier densities p and n are evaluated using the conventional semiconductor expressions along with the *ab initio* density of states of the host material, with a scissors operator applied to give the experimental band gap.

B. Chemical Potentials

The atomic chemical potentials, μ_j , on the right hand side of Eq. 1 are closely related to the experimental growth conditions. A high value of chemical potential of a particular atomic species is equivalent to a growth environment that is rich in that species (in the sense of high partial pressure).

The chemical potentials of Ti and O which enter into Eq. 1 are not independent: equilibrium between the Ti and O atomic reservoirs and bulk TiO_2 anatase requires that

$$\mu_{\text{Ti}} + \mu_{\text{O}_2} = \mu_{\text{TiO}_2}, \quad (4)$$

where μ_{TiO_2} is the total energy of bulk anatase. Moreover, in order to preclude the precipitation of bulk hcp Ti or O_2 dimers there are additional thermodynamic restrictions on the individual chemical potentials:

$$\mu_{\text{O}} < \mu_{\text{O}}^0, \quad (5)$$

and

$$\mu_{\text{Ti}} < \mu_{\text{Ti}}^{\text{bulk}}, \quad (6)$$

where μ_{O}^0 is the energy per atom in an O_2 dimer in its spin triplet ground state and $\mu_{\text{Ti}}^{\text{bulk}}$ is the energy per atom in hcp Ti. It is conventional to refer to the upper limit in Eq. 5 as the O-rich limit and, similarly, to the upper limit in Eq. 6 as the Ti-rich limit. Because of the relationship between μ_{Ti} and μ_{O} in Eq. 4, there are only two independent variables in this approach: the O and Co chemical potentials. This explains why the Ti chemical potential does not enter explicitly into Eq. 3.

Thus, for a given choice of μ_{Co} and μ_{O} , all the other quantities (including E_F) in Eq. 3 are completely determined. In practice, we eliminate μ_{Co} as an independent variable by constraining the total Co concentration to a typical experimental value (5%). Hence, in our formulation, the concentration of all defects is entirely determined by the choice of O chemical potential and the constraint of total Co concentration.

C. Temperature

Although temperature appears in both Eq. 1 (implicitly) and Eq. 2 (explicitly), our results are not especially sensitive to this variable. Moreover, we stress that the temperature appearing in Eq. 2 has no connection to the magnetic ordering temperature, and should instead be understood simply as the temperature at which we evaluate the concentration of defects in equilibrium with their respective reservoirs. Upon completion of growth, we consider the reservoirs to be disconnected and hence the number of these constituents to be fixed. Thus we set the temperature to a particular value and examine the behavior of the system as a function of the O chemical potential. To this end, we calculate the defect concentrations using a typical growth temperature of 873 K.^{1,2,7}

D. Computational Details

The total energy calculations were performed in a supercell consisting of a $3 \times 3 \times 2$ periodic repetition of the primitive unit cell; thus, for the pure TiO_2 host, these supercells contain 108 atoms. Structural relaxation was performed within a sphere of radius of 4 Å centered on the defect in question; calculations using a sphere radius of 5 Å give the same total energy to within 50 meV. This approach has proven both efficient and accurate for other similar metal-oxide insulators.¹⁹ The total energy calculations were evaluated in the local-density approximation (LDA) within the ultrasoft pseudopotential formalism²¹ as implemented in the VASP code,²² with the zone center used to sample the Brillouin zone of the supercells. A kinetic-energy cutoff of 400 eV was used in all total energy evaluations. Only defects involving Co atoms were treated in a spin-polarized fashion. The ground state of bulk hcp Ti was treated non-magnetically, bulk hcp Co was treated in an ferromagnetic configuration, and the total energy of the $\phi 2$ reference dimer was evaluated for the spin triplet.

Since the Fermi energy in Eq. 1 is measured with respect to the VBM of the host, we must align the VBM in the charged defect supercell with that of the host material. To this end, we used a local site average of the electrostatic potential to define a reference energy; this local average was evaluated by a test charge approach in which we calculate the electrostatic energy of a narrow Gaussian charge distribution far from the defect. We

have checked that using, as an alternative, the Ti $3p$ semi-core eigenvalues gives very similar results. Including the zone sampling, kinetic-energy cutoff, lattice relaxation and choice of reference energy, we estimate the numerical uncertainty in our results to be 100–150 meV, sufficient for addressing trends with respect to growth conditions.

To compute the total energy of a charged periodic system, we use a standard procedure which systematically corrects for the artificial and slowly converging Coulomb interaction between charged defects.^{23,24} A neutralizing homogeneous background charge density is first added to the total charge density; this makes the total energy a well-defined quantity. Next, the artificial interaction among the charged defects within this neutralizing background is subtracted from the total energy; this interaction is estimated by expanding the defect-induced electron density in a multipole series up to quadrupole order and then computing the contribution to the total energy from the interaction of these multipoles.²⁵

Finally, we note that although the electronic band gap does not enter explicitly into Eq. 1, the LDA underestimation of the gap does affect the formation energies of shallow donors, such as O vacancies and interstitial Co. We have observed, however, that the depths of these donor levels (relative to the conduction-band edge) are essentially independent of the value of the band gap. We demonstrated this by calculating the position of the donor level using an artificially reduced lattice constant; as the band gap increases with decreasing lattice constant, the donor level closely tracks the conduction-band edge. Thus, we have corrected the formation energies of these donors using the experimental value of the band gap and the depth of the donor levels given within LDA. In addition, we assume that the LDA correctly predicts the formation energies of the +2 charge states of these defects, because all defect levels are empty in this charge state.

IV. RESULTS AND DISCUSSION

A. Electronic Structure of Co_{Ti}

We discuss first the electronic structure of the isolated substitutional Co dopant. Fig. 1(a) shows the single-particle levels of neutral substitutional Co, as determined from the eigenvalue spectra at $k = \Gamma$ using a 108-atom supercell. The point group for this defect is D_{2d} , so that all but one of the $3d$ -orbital degeneracies are lifted by the crystal field; nevertheless, the environment surrounding the Co dopant is still very nearly cubic, so that the e_g and t_{2g} parentage of these levels is easily seen. There are 3 occupied majority-spin levels and 2 occupied minority-spin levels, yielding a net magnetic moment of $1 \mu_B$.

It is instructive to study separately the exchange splitting and crystal-field splitting. This separation occurs naturally in the $q = -1$ charge state, for which the exchange splitting vanishes, as shown in Fig. 1(b). In this

case the largest crystal-field splitting, about 1 eV, is between the e_g and t_{2g} manifolds, with the e_g manifold near the LDA conduction-band edge and the t_{2g} near the valence-band edge. The D_{2d} crystal field further splits the e_g manifold into an upper a_1 level of z^2 symmetry and a lower b_1 level of $x^2 - y^2$ symmetry; this splitting is 0.3 eV. Likewise, the crystal field splits the t_{2g} manifold into an upper b_2 level of xy symmetry and a two-fold e level of (xz, yz) symmetry; this splitting is 0.2 eV.

For charge states with non-zero magnetic moments, we find that the exchange splitting varies approximately linearly with the magnetic moment. (Since the orbital moment is strongly quenched,²⁶ we regard the magnetic and spin moments as equivalent.) For neutral substitutional Co, the exchange splitting within the e_g manifold is 0.2 eV for both levels. Within the t_{2g} manifold, the exchange splitting is strongly orbital-dependent: 0.5 eV for the b_2 levels and 0.3 eV for the e levels.

The calculated magnetic moments of substitutional Co in different charge states, summarized in Table I, can now be easily understood from the results of Fig. 1. For the neutral substitutional, there is a two-fold degenerate half-filled minority spin level at the Fermi level. Removing an electron from this level leads to a +1 charge state with a moment of $2 \mu_B$. Likewise, adding an electron to this level leads to a -1 charge state with zero moment, since the t_{2g} manifold is now completely filled.

The stable charge states and magnetic moments for interstitial Co are quite different from the substitutional case. For example, we find that all charge states experience off-center structural relaxations of order 1 Å, lifting all remaining orbital degeneracies. The +2 charge state of interstitial Co, which is the lowest-energy charge state over most of the gap, has a moment of $1 \mu_B$. The +1 charge state leads to a moment of $2 \mu_B$, whereas the neutral configuration has a moment of $1 \mu_B$.

B. Oxidation State

Since the correspondence between “formal oxidation state” and “charge state” will be an important issue here, we briefly summarize the relationship between the two. A similar discussion has been given for transition-metal impurities in GaP.¹⁶ When a neutral Co substitutes for Ti in TiO₂, it takes on the oxidation state IV, the same as that of Ti. Hence a substitutional Co_{Ti} in the -1 charge state has a formal oxidation state of III, and a substitutional Co_{Ti} with charge -2 has an oxidation state of II. In a similar fashion one can relate the oxidation state and charge state of interstitial Co; in this case however, the charge state of the dopant is the same as the oxidation state. Hence, neutral interstitial Co has oxidation state 0, the charge state +1 has oxidation state I, and so forth. The oxidation state of Co-related dopants in their various stable charge states are summarized in Table I.

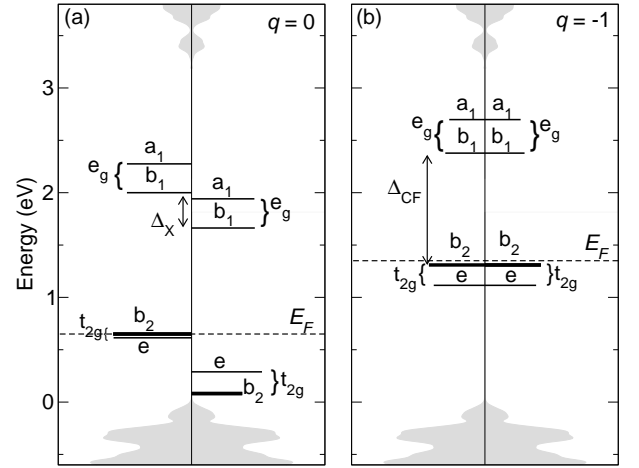


FIG. 1: First-principles energy-level diagram for substitutional Co_{Ti} in TiO₂ anatase. (a) Neutral charge state; (b) Singly charged state, $q = -1$. The density of states of the anatase host is shown as the gray shaded regions with a scissors operator applied to give the experimental band gap. The length of each impurity level is proportional to its d character. The exchange splitting, Δ_X , and crystal field splitting, Δ_{CF} , are discussed in Sec. 4(c) (see text).

TABLE I: Stable charge states of various Co dopants in TiO₂ anatase, with their formal oxidation states and calculated magnetic moments. The results for the -2 charge state of Co_{Ti} are obtained from a model described in the text. The oxidation state values in parentheses for Co_{Ti}V_O complexes are based on the assumption that the neutral complex can be represented as Co_{Ti} and V_O in the -2 and +2 charge states, respectively.

Defect	Charge	Oxidation state	M (μ_B)
Co _{Ti}	1	V	2.0
	0	IV	1.0
	-1	III	0.0
	-2	II	1.0
Co _{int}	2	II	1.0
	1	I	2.0
	0	0	1.0
Co _{Ti} V _O -c	1	-	2.0
	0	(II)	1.0
Co _{Ti} V _O -ab	1	-	0.0
	0	(II)	1.0

C. The -2 Charge State of Co_{Ti}

In the LDA calculation there is no stable -2 charge state of substitutional Co: upon adding an additional electron to the stable -1 charge state, we find no dopant-derived level within the gap, but rather partial occupation of the LDA conduction bands. This is problematic, since the experimental finding of an oxidation state of

II for Co would be consistent with a -2 charge state for substitutional Co. Here we investigate whether the absence of a -2 charge state within LDA is due to the well-known underestimation of the band gap by the LDA (the LDA predicts a band gap of 2.2 eV compared to the experimental value of 3.2 eV²⁷).

Rather than attempting to correct the LDA band gap, we propose a more direct description and try to estimate the formation energy of the -2 charge state using our results for the energy levels of the -1 charge state. Since the formation energy is in general a linear function of the Fermi energy, we do this in terms of the “energy of transition,” $E(-/-)$, which is defined as that value of E_F for which $E_{\text{form}}^{q=-1}$ is equal to $E_{\text{form}}^{q=-2}$. Referring to Fig. 1(b), we model the -2 charge state by occupying the first available impurity level in the $q = -1$ level diagram, namely the empty b_1 level. In this diagram, the b_1 level is at $E_F + \Delta_{CF}$, so that occupying it will shift the Fermi level upward by an amount Δ_{CF} . However, by singly occupying this level, one expects an accompanying exchange splitting and thus a downward shift of the Fermi level. Hence, we estimate the change in the Fermi energy between the -1 and -2 charge state to be given by

$$E(-/-) = E(0/-) + \Delta_{CF} - \Delta_X, \quad (7)$$

where $E(0/-)$ is the energy of transition between the neutral and -1 charge states; Δ_{CF} is the crystal-field splitting between the b_2 and b_1 levels; and Δ_X is the exchange splitting due to the unpaired b_1 electron.

We approximate Δ_X by the b_1 exchange splitting for the neutral state; this is 0.3 eV, as shown in Fig. 1(a). We neglect the onsite energy which arises from the interaction of the added b_1 electron with the t_{2g} electrons, but we expect this energy to be significantly smaller than the crystal-field energy, and hence expect Eq. 7 to be reasonably accurate.

A similar proposal could be made for more-negative charge states, for example, the -3 charge state of substitutional Co. However, we should then include an additional term, U , for the onsite interaction between two b_1 electrons of opposite spin. This onsite energy will be large and can be estimated as

$$U \geq E(0/-) - E(+/0) - \Delta_X, \quad (8)$$

where $\Delta_X = 0.3$ eV is again taken from the neutral configuration, but in this case accounts for the exchange energy lost when the moment is reduced from 1 μ_B to zero in the transition from the neutral to the -1 charge state.²⁸ We find $U \geq 1.0$ eV and, hence, the -3 charge state of substitutional Co will lie well above the conduction-band edge, so that it (and more highly charged negative states) can be excluded from further consideration.

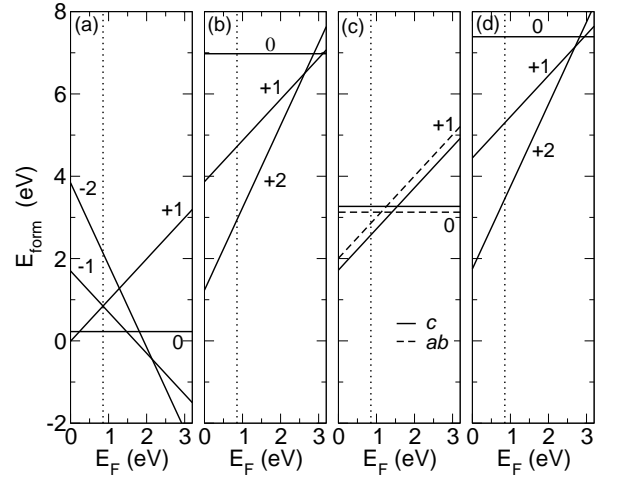


FIG. 2: Formation energies of (a) Co_{Ti} , (b) Co_{int} , (c) $\text{Co}_{\text{Ti}}\text{V}_\text{O}$, (d) V_O defects as a function of Fermi level in the O-rich limit. The Co chemical potential was chosen to give a total Co concentration of 5%. The Fermi energy which satisfies electroneutrality for these choice of growth conditions and Co concentration is denoted by the dotted vertical line. The stable charge states for each defect are labeled.

D. Formation Energies in the O-rich Limit

To address the characteristics of Co-doped samples grown with OPMBE we first consider conditions O-rich growth conditions. Figure 2 shows the defect formation energies versus Fermi energy in the O-rich limit, with the total Co concentration constrained to be 5%. In comparison to experiment this scenario has three main shortcomings: (1) the average magnetic moment is 1 μ_B , significantly smaller than the measured value^{3,4} of 1.26 μ_B ; (2) the Fermi level is well below midgap, whereas experimental measurements show the material to be n -type;^{1,4,14} (3) Co appears almost entirely as neutral substitutionals (oxidation state IV), whereas Co 2*p* photoemission and XANES suggest the oxidation state of Co is II.^{4,14} These discrepancies suggest that the conditions present during growth of the samples are not O-rich.

E. Variation with O Chemical Potential

To determine what growth conditions give rise to the observed magnetic and transport properties of Co-doped anatase samples, we study the consequences of varying the O chemical potential away from its upper limit. In Fig. 3 we plot, versus the O chemical potential, the following quantities: concentration of substitutional and interstitial Co; n and p carrier densities; average magnetic moment per Co; percentage of Co in different oxidation states; and concentration of O vacancy-related defects (the concentration of interstitial Ti is negligible throughout this range of O chemical potential). For every

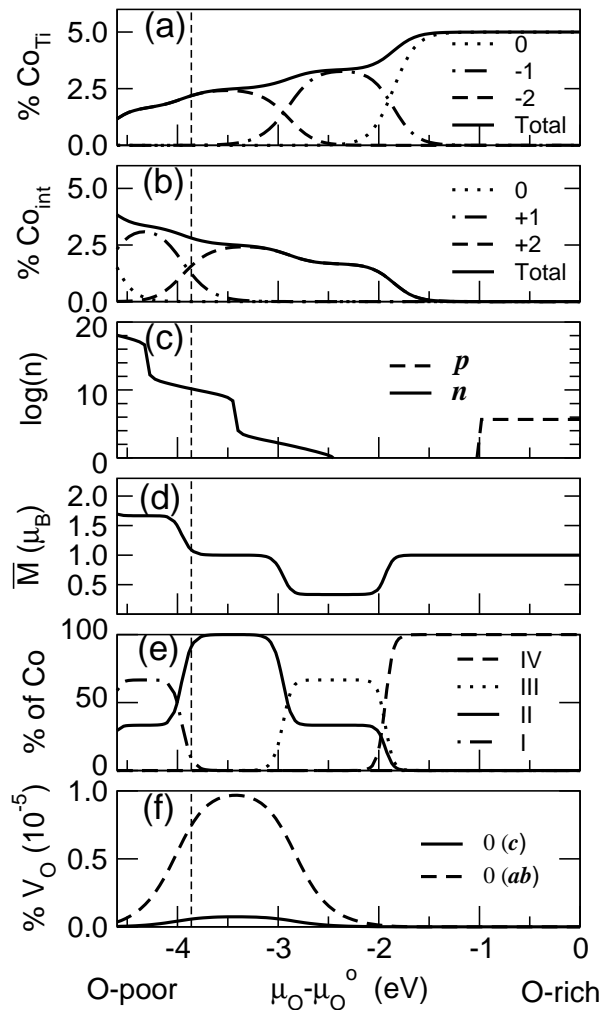


FIG. 3: Variation, versus O chemical potential, of (a) Co_{Ti} concentration, (b) Co_{int} concentration, (c) carrier concentration, (d) average magnetic moment per Co, (e) percent of Co in various oxidation states, and (f) concentration of V_{O} -related defects versus O chemical potential. In panels (a) and (b) the concentration of each charge state of Co is indicated as well as the total concentration. In panel (f) only the concentration of $\text{Co}_{\text{Ti}}\text{V}_{\text{O}}$ defects are shown, since the concentration of isolated O vacancies is much smaller. Values of the O chemical potential to the left of the dashed vertical line are those for which our theoretical results agree qualitatively with experiment (see text).

value of the O chemical potential, the total concentration of Co was constrained to 5%.

1. Cobalt concentration

For values of the O chemical potential within ~ 1.5 eV of the O-rich limit, the substitutional site remains the

preferred Co site. The situation is very different in the O-poor limit. In this regime, interstitial Co (in the +1 and +2 charge states) becomes energetically competitive with substitutional Co, and hence the concentrations of substitutional and interstitial Co become comparable. This results from a subtle balance of the O and Co chemical potentials. As one decreases the O chemical potential from its upper limit, the formation energies of substitutional dopants increases, since it costs more energy to replace Ti with Co as one moves toward the Ti-rich limit. Of course, as a function of the O chemical potential, the Co chemical potential must also change, increasing monotonically to maintain the fixed total Co concentration. At ~ 1 eV below the O-rich limit, interstitial Co begins to play a role; the preference for the interstitial site increases monotonically below this point, eventually accounting for most of the total Co concentration in the O-poor limit.

2. Carrier densities

The defect concentrations shown in Fig. 3 were computed for a temperature of 873 K, as mentioned earlier. However, since transport, magnetometry, and photoemission measurements are generally performed at room temperature, we have used a more relevant temperature of 300 K to compute the carrier concentrations, magnetic moments, and oxidation-state fractions—while keeping the total defect concentrations themselves frozen at their high-temperature values.

Figure 3(c) shows the logarithm of the hole and electron carrier densities evaluated at 300 K as a function of the O chemical potential. Near the O-rich limit the carrier densities are nearly constant, since the Fermi level maintains a value of ~ 0.8 eV relative to the VBM due to compensation by equal but small numbers of substitutional Co in the -1 and $+1$ charge states. In this region the material is very weakly p -type with a hole concentration $\sim 10^6/\text{cm}^3$ and will likely appear insulating in transport measurements.

At ~ 1 eV below the O-rich limit, the appearance of interstitial Co leads to partial compensation of the Co substitutional defects. This compensation drives the Fermi level towards the conduction-band edge, and leads to a marked increase in the electron concentration as the O chemical potential is further reduced. The step-wise behavior of the carrier density as the O chemical potential is decreased results from the Fermi level passing through donor levels due to interstitial Co. At the O-poor limit, we find $n \sim 10^{20}/\text{cm}^3$. Thus, we suggest that the experimentally observed n -type behavior results from the incomplete compensation of interstitial Co by substitutional Co, which facilitates the thermal excitation of electrons from interstitial Co into the conduction band.

3. Magnetic moment

In Fig. 3(d) we show the average magnetic moment per Co, defined here as

$$\overline{M} = \sum_{D,q} M_D^q C_D^q / \sum_{D',q'} C_{D'}^{q'}, \quad (9)$$

where M_D^q is the magnetic moment of a Co-related defect in charge state q . We assume a ferromagnetic alignment of all the moments, and thus \overline{M} can be considered an upper bound for the measured average value of the moment per Co.

The average moment shows a non-monotonic variation with O chemical potential. In the O-rich region it is constant with a value of $1 \mu_B$, because neutral substitutional Co is the dominant defect. For intermediate values of the O chemical potential, \overline{M} is less than $1 \mu_B$ due to the presence of substitutionals in the -1 charge state, which have zero moment. In the O-poor limit the average moment per Co is larger than $1 \mu_B$, due to the appearance of interstitial Co in the $+1$ charge state, which has a moment of $2 \mu_B$. Hence, only in the O-poor limit do we obtain a moment per Co larger than the Co^{2+} low-spin value of $1 \mu_B$, and thus consistent with experiment.

4. Oxidation states

Figure 3(e) shows the percentage of Co dopants in different oxidation states. In the O-rich limit the oxidation state of Co is IV, since it occurs primarily as a neutral substitutional. This oxidation state dominates until ~ 1.5 eV below the O-rich limit where oxidation state III, resulting from substitutionals in the -1 charge state, is briefly dominant. Between 3 and 4 eV below the O-rich limit the predominant oxidation state of Co is II, the same as that deduced from the $2p$ photoemission and XANES results of Refs.4 and 14. In the O-poor limit the oxidation state is primarily I, since the dominant type of defect is interstitial Co in the $+1$ charge state. Although this oxidation state has not been observed experimentally, comparison to photoemission or XANES results on samples with known Co oxidation state of I has not been established.

5. O vacancies

For all thermodynamically allowed chemical potentials, the concentration of isolated O vacancies is negligible, as well as that of CoTiV_O complexes; their concentrations are shown in Fig. 3(f) to be never above $10^{-5} \%$. These low concentrations result from the fact that the formation energies of these two defects are much higher than the thermal energy $k_B T = 60$ meV; this is clear from Fig. 2, where the formation energy of both isolated V_O and CoTiV_O complexes is greater than 2 eV for any value

of the Fermi level. Thus O vacancies, either isolated or in complexes with substitutional Co, will play no significant role in determining the carrier concentration in Co-doped samples.

We note that the formation energies of O vacancies in Fig. 2 and the deduced donor level positions in the band gap are incompatible with the interpretation of the observed n -type conductivity of pure TiO_2 samples.¹⁰ Even in the O-poor limit, the LDA does not lead to a carrier density with the observed value $10^{18}/\text{cm}^3$, nor does it give the same temperature dependence of the carrier concentration, as the energy for activation is quite different: ~ 200 meV (the position of the highest O vacancy donor level below the conduction band edge) in the LDA versus 4.2 meV in the results of Ref. 10. We do not have a definitive resolution to this apparent disagreement; we have checked, however, that if we adjust the O vacancy formation energies to reproduce the experimentally observed carrier density and temperature dependence in undoped samples, the conclusions of this work are unchanged.

Regarding the experimental interpretation that O vacancies are also the source of n -type carriers in Co doped samples,^{3,4} we note that the observed average moment per Co of $1.26 \mu_B$ can only be reproduced if some fraction of Co interstitials in the $+2$ charge state are present, as only these defects have a moment larger than $1 \mu_B$. Neither substitutional nor interstitial Co has any significant orbital moment²⁶ so that the observed magnetic moment per Co can only result from the statistical distribution of Co moments in interstitial ($2 \mu_B$) and substitutional ($1 \mu_B$) sites. In such a situation the Fermi level and carrier concentration are determined solely by the Co dopants.

6. Conclusion

Considering these trends in the n -type carrier density, average magnetic moment per Co, and oxidation state of Co, we suggest the actual conditions of growth of Co-doped TiO_2 anatase are O-poor, corresponding to O chemical potentials between 3.8 and 4.6 eV below the O-rich limit (values of the O chemical potential to the left of the dashed vertical line in Fig. 3). Under these type of conditions we obtain qualitatively and quantitatively good agreement with experimental observations.

V. SUMMARY

In summary, we have examined the role of native defects and Co dopants in TiO_2 anatase over a range of chemical potentials corresponding to different growth conditions. Under O-rich growth conditions we find that Co dopants will be formed primarily in neutral substitutional form corresponding to oxidation state IV, an average magnetic moment of $1 \mu_B$ and insulating electrical character. These results are in conflict with the exper-

imentally observed behavior of Co-doped samples and suggest that the growth conditions are more likely to be O-poor. O-poor conditions lead to roughly equal concentrations of substitutional and interstitial Co, n -type behavior resulting from thermal excitation of electrons from interstitial Co into the conduction band, and an average magnetic moment per Co in good agreement with experiment.

Acknowledgments

One of the authors (J.M.S.) acknowledges the National Research Council for support during this work in the

form of a postdoctoral associateship. This work was funded in part by DARPA and ONR. Computational work was supported in part by a grant of HPC time from the DoD Major Shared Resource Center ASCWP.

-
- ¹ Y. Matsumoto, M. Murakami, T. Shono, T. Hasegawa, T. Fukumura, M. Kawasaki, P. Ahmet, T. Chikyow, S. Koshihara, and H. Koinuma, *Science* **291**, 854 (2001).
 - ² S. A. Chambers, S. Thevuthasan, R. F. C. Farrow, R. F. Marks, J. U. Thiele, L. Folks, M. G. Samant, A. J. Kellock, N. Ruzycki, D. L. Ederer, and U. Diebold, *Appl. Phys. Lett.* **79**, 3467 (2001).
 - ³ S. A. Chambers, *Materials Today* **April**, 34 (2002).
 - ⁴ S. A. Chambers, S. M. Heald, R. F. C. Farrow, J.-U. Thiele, R. F. Marks, M. F. Toney, and A. Chattopadhyay, *cond-mat/0208315* (2002).
 - ⁵ S. R. Shinde, S. B. Ogale, S. Das Sarma, S. E. Lofland, C. Lanci, J. P. Buban, N. D. Browning, V. N. Kulkarni, J. Higgins, R. P. Sharma, R. L. Greene, and T. Venkatesan, *cond-mat/0203576* (2002).
 - ⁶ J. R. Simpson, H. D. Drew, S. R. Shinde, Y. Zhao, S. B. Ogale, and T. Venkatesan, *cond-mat/0205626* (2002).
 - ⁷ I.-B. Shim, S.-Y. An, C. S. Kim, S.-Y. Choi, and Y. W. Park, *J. Appl. Phys.* **91**, 7914 (2002).
 - ⁸ Y. L. Soo, G. Kioseoglou, S. Kim, Y. H. Kao, P. Sujatha Devi, J. Parise, R. J. Gambino, and P. I. Gouma, *Appl. Phys. Lett.* **81**, 655 (2002).
 - ⁹ M. S. Park, S. K. Kwon, and B. I. Min, *Phys. Rev. B* **65**, 161201(R) (2002).
 - ¹⁰ L. Forro, O. Chauvet, D. Emin, L. Zuppiroli, H. Berger, and F. Levy, *J. Appl. Phys.* **75**, 633 (1994).
 - ¹¹ Y. D. Park, A. T. Hanbicki, S. C. Erwin, C. S. Hellberg, J. M. Sullivan, J. E. Mattson, T. F. Ambrose, A. Wilson, G. Spanos, and B. T. Jonker, *Science* **295**, 651 (2002).
 - ¹² H. Ohno, *Science* **281**, 951 (1998).
 - ¹³ T. Dietl, H. Ohno, F. Matsukura, J. Cibert, and D. Ferrand, *Science* **287**, 1019 (2000).
 - ¹⁴ S. A. Chambers (private communication).
 - ¹⁵ S. A. Chambers, *Solid State Commun.* **39**, 105 (2000).
 - ¹⁶ V. A. Singh and A. Zunger, *Phys. Rev. B* **31**, 3729 (1985).
 - ¹⁷ S. B. Zhang, S.-H. Wei, A. Zunger, and H. Katayama-Yoshida, *Phys. Rev. B* **57**, 9642 (1998).
 - ¹⁸ C. G. Van de Walle, *Phys. Rev. Lett.* **85**, 1012 (2000).
 - ¹⁹ A. F. Kohan, G. Ceder, D. Morgan, and C. G. Van de Walle, *Phys. Rev. B* **61**, 15019 (2000).
 - ²⁰ P. Mahadevan and A. Zunger, *Phys. Rev. Lett.* **88**, 047205 (2002).
 - ²¹ D. Vanderbilt, *Phys. Rev. B* **41**, 7892 (1990).
 - ²² G. Kresse and J. Fürthmüller, *Phys. Rev. B* **54**, 11169 (1996).
 - ²³ G. Makov and M. C. Payne, *Phys. Rev. B* **51**, 4014 (1995).
 - ²⁴ L. N. Kantorovich, *Phys. Rev. B* **60**, 15476 (1999).
 - ²⁵ We assume that the monopole-quadrupole interaction energy in a tetragonal cell is of the same form as that for a simple cubic cell.²³ This assumption is confirmed by calculations of atomic ionization energies in tetragonal supercells of the same size and shape as that of our defect supercells.
 - ²⁶ J. M. Sullivan and S. C. Erwin (unpublished).
 - ²⁷ T. Tang, H. Berger, P. E. Schmid, F. Levy, and G. Burri, *Solid State Commun.* **23**, 161 (1977).
 - ²⁸ We assume this is a lower bound, since the e_g orbitals are more localized than the t_{2g} orbitals, and thus can be expected to have a larger onsite interaction.